

# Study on the Potent Binding of Anti Cancerous Drug Binding Using Various Spectroscopic and Computational Techniques

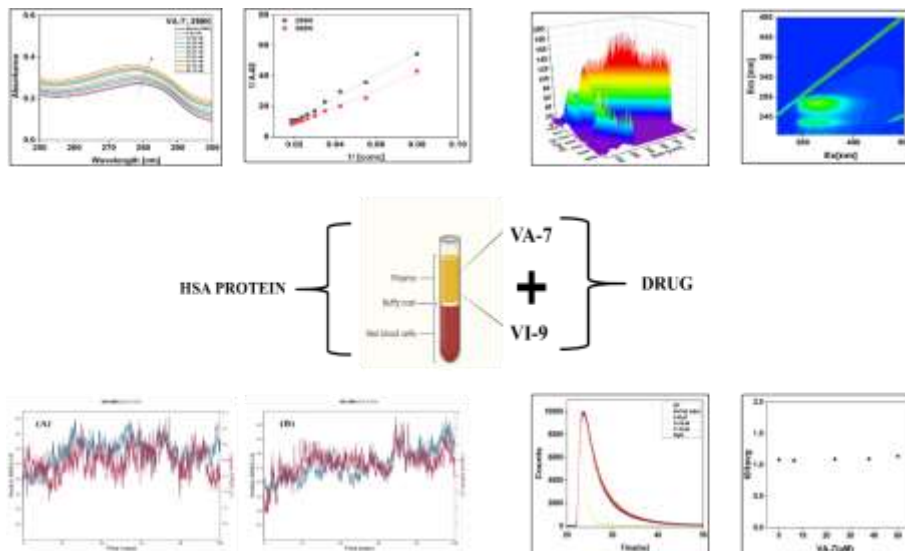
Ms. Neha Neha

## ABSTRACT

An alarming number of people worldwide lose their lives to cancer every year. Anticancer medications are used to treat malignant growths or malignancies in the human body. Because human serum albumin [HSA] is a protein that is present in human blood and has the ability to bind, it is in charge of delivering a variety of medications to the relevant body areas. The purpose of this work is to investigate the binding of HSA to VA-7/VI-9 as an anti-cancer medication. A number of thermodynamics parameters need to be determined. Overall, the binding interaction process's conformational and structural modifications, binding constant, Vander Waal forces, and binding energy were defined in the current work. Numerous computational methods and spectroscopic techniques were employed to bind anti-cancer drugs to HSA. The thermodynamic parameters involved in the binding process are estimated using circular dichroism (CD) and molecular docking.

**KEYWORDS:** Cancer, Anti-cancerous, Human Serum Albumin, HSA binding, Interaction.

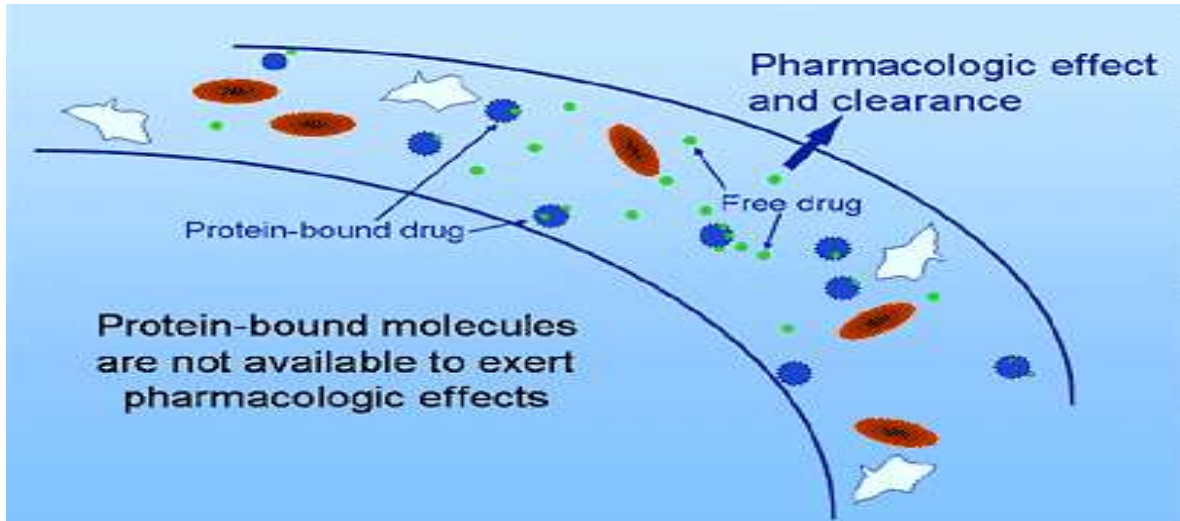
## GRAPHICAL ABSTRACT



## INTRODUCTION

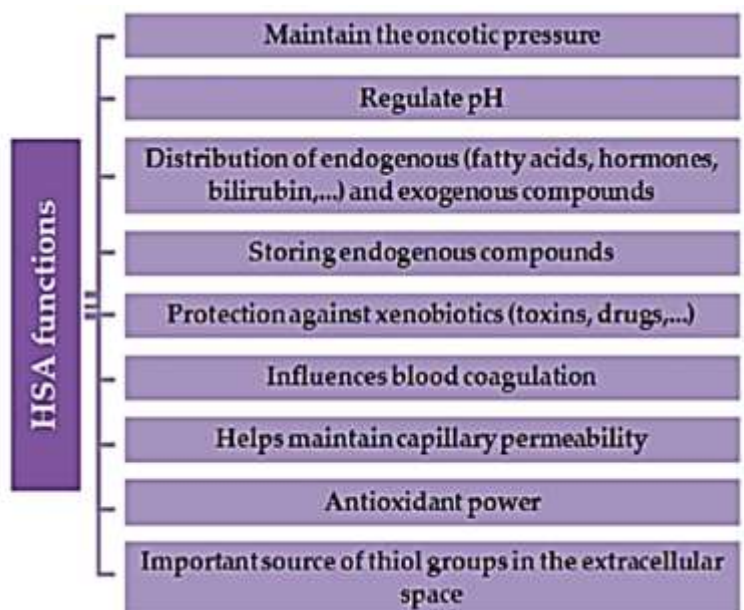
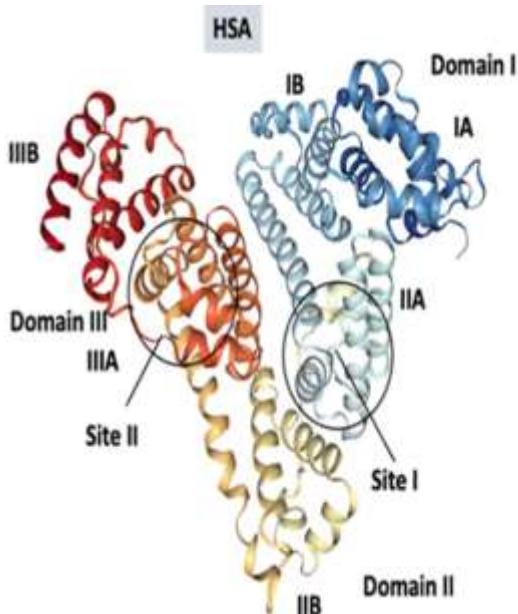
When the drug bind with protein is commonly referred as drug binding interaction. Here, protein act as a carrier which carry the drug from the blood and distribute it to the various parts or organ of the human body. Drug binding is a reversible process as after binding it form a drug protein complex and release the

drug to its target site. There are two regions in which different type of proteins are present i.e. vascular region [plasma protein], extravascular region [tissue, organ].



### VARIOUS FACTORS AFFECTING PROTEIN-DRUG BINDING

- **Drug related factor**
  - total concentration of drug in the body.
- -affinity of drug binding with the component.
- **The protein**
  - quantity of the drug for binding with protein.
  - binding sites on protein.
- **Drug interaction**
  - competition with endogenous components.
- **Patient related factor**
  - age factor.
  - physiological condition.



In the drug development, serum albumin alters the drug’s therapeutic efficacy. While studying this process understanding binding interaction with HSA is critical. Human serum albumin [HSA] is a non – toxic and non – antigenic plasma protein. Its interaction with drug directly form a ‘Nano drug’ increasing drug availability. HSA has seven long-chain fatty acid binding sites throughout the three homologous domains I, II, III. Each domain contains two sub – domain [A and B], which contains 4 and 6 alpha-helices. Albumin is a most abundant drug found in plasma. It covers half of the total blood present in the human body. The concentration of albumin in plasma of human healthy body is 3.5-5 g/dl. Albumin is synthesized by liver hepatocytes cells but very little amount is present in liver. We consider HSA to maintain oncotic pressure in the human body.

Anti-cancerous drug kills or modify growth . Chemotherapy is medication that is used to destroy, kill, shrink, or slow the growth of cancer cells. Discovery of anti-cancerous agents started after 1940. Cancer treatment: -chemotherapy, radiotherapy, immunotherapy, surgery. Anti-cancerous drugs are classified as cytotoxic, targeted and hormonal drug In treatment of cancer, interactions between anticancer drugs and HSA are important as the amount of unbound drug fraction is instantly associated with the actual concentration of the drug at its biological target site. [2]. There are more than 100 different types of cancers, each with its own characteristics, risk factors, and treatment options. In 2020, approximately 18.1 million new cases of cancer were reported worldwide, excluding non-melanoma skin cancer, with 8.8 million (48%) in females and 9.3 million (52%) in males. This resulted in a ratio of 10 males to every 9.5 females. The global age-standardized incidence rate was 178.1 per 100,000 females and 206.9 per 100,000 males [1]. In 2020, the FDA approved 18 new cancer drugs, including the HER2-directed margetuximab, sacituzumab govitecan [a TROP2-targeted antibody–drug conjugate (ADC) for triple-negative breast cancer] and the BCMA-targeted ADC belantamab mafodotin for multiple myeloma [3].

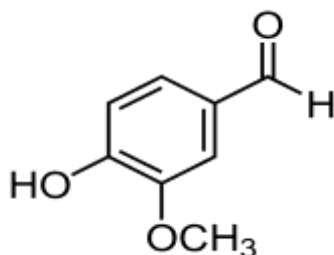
**Various natural compounds used as anti-cancer treatments in treating various cancers via different pathways.**

Name Of Compound	Source	Mechanism Of Action	Cancer	Reference
Vinblastine	Periwinkle plant (Catharanthus rose us)	Inhibits microtubule assembly	Breast, colorectal, lung, ovarian, prostate	[4]
Vincristine	Periwinkle plant (Catharanthus rose us)	Binds to tubulin, inhibits microtubule formation	Liver.	[5]
Curcumin	Turmeric (Curcuma longa)	Inhibits cell proliferation, induces apoptosis.	Breast, lung, skin, gastrointestinal, colorectal, prostate, head and neck	[6]
Berberine	Berberi’s plants	Inhibits cell progression, promotes apoptosis.	Colon.	[7]

### Parent Compound: - Vanillin

Vanillin (chemical name: 3-methoxy-4-hydroxy benzaldehyde), the parent compound of VA-7/VI-9 has large variety of application in research field. Vanillin is widely used as aroma compound in foods, beverages, pharmaceuticals and daily chemicals. Natural vanillin is produced by bioconversion and physical methods from the cured fruit of orchid plant. Besides its flavour qualities, vanillin possesses interesting biological properties such as anti-mutagenic nontoxicity, antimicrobial potential and large availability. Therefore, it is extensively used as a source biomaterial in food Industries [8].

### Chemical Structure of parent Compound Vanillin.

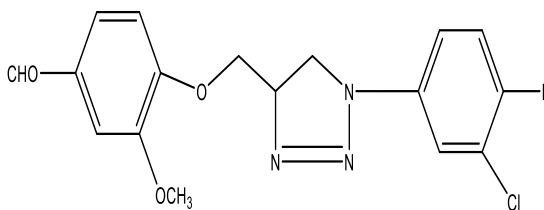


Chemical Formula: - C<sub>8</sub>H<sub>8</sub>O<sub>3</sub>

Molecular Weight: - 152.15 g/Mol

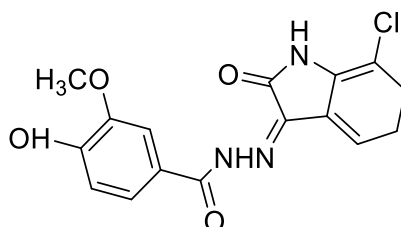
### Compound Information

#### VA-7



- IC<sub>50</sub> > 10 μM
- K<sub>a</sub> = 0.7 × 10<sup>3</sup> (M<sup>-1</sup>)
- Molecular weight = 327.32 Da

#### VI-9



- K<sub>b</sub> = -8.6 KJ/Mol
- Molecular weight = 345.74 Da

The function of HSA is responsible for the transport and distribution of metabolism and excretion of drugs. Drug distribution is mainly controlled by HSA, because most drugs travel in the plasma and reach their target tissues by binding to HSA. Therefore, studies of protein–drug interactions are widely used, as it

provides information on the conformational changes that determine the therapeutic effectiveness of drugs, and become an important research field in the life sciences, chemistry and clinical medicine. In this paper, the interaction between VA-7/VI-9 and HSA has been studied for first time using multi-spectroscopic (fluorescence, UV/vis absorption, steady state fluorescence, synchronous fluorescence, 3D fluorescence, time resolve fluorescence (TRF), isothermal calorimetry (ITC), circular dichroism (CD) and molecular docking (MD) techniques. Also, the binding constant ( $K_b$ ), thermodynamics parameters and the effect of VA-7/VI-9 on the protein conformation for the reaction were determined. Furthermore, the mechanism of VA-7/VI-9 binding to HSA was proposed and discussed here for the molecular modelling method.

## EXPERIMENTAL

### Materials and Methodology

HSA was purchased from Sigma-Aldrich [USA]. The stock solution of HSA was prepared by directly dissolving protein in phosphate buffer of pH 7.4. Solutions were then stored in the refrigerator at 4°C. For making stock of drug [VA-7/VI-9] we have to weigh the compound on electronic weighing machine and dissolve it in new Eppendorf in DMSO (dimethyl sulfoxide). [Molecular weight = 78.13 g/Mol; purity 99.0%]. After that we prepared the working solution by dissolving it into an ultra-pure water. For HSA – VA-7/VI-9 binding study, different concentrations of VA-7/VI-9 [6.45-69.56  $\mu$ M] were used. Millipore water was used throughout the experiment.

### UV- vis SPECTROSCOPY

For monitoring the absorption spectrum of HSA, Analytik Jena Specord-210 spectrophotometer [Germany] was used. The absorbance spectrum was recorded by keeping the concentration of HSA [5  $\mu$ M] with varying concentration of VA-7/VI-9. It is generally used to determine the absorption spectrum of HSA. In this technique the sample whose absorption is to be determined is put in the cuvette of 1 cm path length and placed in a sample holder with a reference constant concentration (5  $\mu$ M) placed in a sample reference holder. The light was passed from left to right in the spectrometer and we can calculate the absorption spectrum using Beer Lambert Law. The detector detects the absorption spectra line within a wavelength of 200nm to 400nm. All measurement are performed at two temperatures i.e. 298K & 308K. The absorbance of protein without drug is determined at highest peak of wavelength 279 nm and from absorbance value we can calculate the molar concentration of protein [HSA].

### Principle behind the UV-vis spectroscopy is Beer Lamberts Law: -

The concentration of the sample is obtained by determining the absorbance of this sample at specific wavelength by the equation-

$$A = -\log T = -\log (I/I_0) = \log(I_0/I) = \epsilon \cdot c \cdot l$$

$$A = \epsilon \cdot c \cdot l$$

Where A = absorbance

l = optical path length of the cell or cuvette or sample holder (cm)

c = concentration of the solution (Mol dm<sup>-3</sup>)

$\epsilon$  = molar absorptivity of the compound or molecule in solution, which is constant for a particular substance at a particular wavelength [36,500 dm<sup>3</sup> mol<sup>-1</sup> cm<sup>-1</sup>]

Reference [buffer] in a cuvette gives the transmittance vs wavelength graph. Drug with HSA in a cuvette gives the absorbance vs wavelength graph.

### STEADY – STATE FLUORESCENCE

For fluorescence measurement, Cary Eclipse spectrofluorometric [Varian, HSA] equipped with a 150W xenon lamp was used. Fluorescence spectra of HSA [(5 $\mu$ M) in the absence and presence of different concentration of VA-7/VI-9 [6.45-69.56 $\mu$ M] were measured at 298K in a wavelength range of 300-600 nm. The excitation wavelength was set at 210 nm and temperature was set at 298K with cell holder connected to constant temperature water circulator [Varian, USA]. The excitation and emission slit width was set at 5 nm.

### SYNCHRONOUS FLUORESCENCE

The synchronous fluorescence measurement was performed by keeping the difference between excitation and emission wavelength [ $\Delta\lambda = \lambda_{em} - \lambda_{ex}$ ] at a constant temperature of 298K. Synchronous fluorescence spectra was monitored at  $\Delta\lambda = 15$  nm and 60 nm that gives the characteristics information about the binding efficiency of VA-7/VI-9 with Tyrosine [Tyr] and tryptophan [Trp] residues, respectively. The emission was recorded in the range of 200-400 nm for both Tyr and Trp with both the excitation and emission slit widths of 5nm.

### THREE –DIMENSIONAL (3D) FLUORESCENCE

The 3D fluorescence spectra of HSA [5  $\mu$ M] in the absence and presence of VA-7/VI-9 [50  $\mu$ M] were obtained at 298K. The  $\lambda_{ex}$  range was set from 200 to 500 nm, with an increment of 5nm. The emission spectra were successively recorded between 200-500 nm. Both the excitation and emission slit widths for 3D model were set at 5 nm. The experimental temperature was maintained by using a constant – temperature cell holder connected to a constant temperature water circulator [ Varian, USA].

### TIME – RESOLVE FLUORESCENCE SPECTROSCOPY

For monitoring fluorescence lifetime decay profiles, the time – correlation single – photon counting spectrometer equipped with pulsed nanosecond light emitting diode (LED) excitation heads at 279 nm (Horiba, UK) was used. The excitation and emission wavelengths were set at 279 nm and 330 nm, respectively. The instrumental response function (IRF) was recorded sequentially using a scattering solution and a time calibration of 0.050 ps/ channel. The measurement was performed at 298K with the sample added in 1 cm path length quartz cuvette placed in thermostatic holder. The goodness of fit was confirmed in terms of chi- square ( $\chi^2$ ) value and weighted residuals.

### MOLECULAR DOCKING

Molecular docking of VA-7 and VI-9 with HSA was performed to predict their binding affinity and detailed interactions. The docking was performed using InstaDock, a single click molecular docking tool that automizes the entire process of molecular docking-based virtual screening [9]. The binding affinities between the ligand and protein were calculated using the QuickVina-W [10] (Modified AutoDock Vina [11]) program which uses a hybrid scoring function (empirical + knowledge-based) in docking calculations and a blind search space for the ligand.

The  $pK_i$ , the negative decimal logarithm of inhibition constant [12] was calculated from the  $\Delta G$  parameter while using the following formula:

$$\Delta G = RT(\text{Ln } K_{i\text{pred}})$$

$K_{i_{pred}} = e^{(\Delta G/RT)}$   $pKi = -\log(K_{i_{pred}})$  where  $\Delta G$  is the binding affinity ( $\text{kcal mol}^{-1}$ ),  $R$  (gas constant) is  $1.98 \text{ cal} \cdot (\text{mol} \cdot \text{K})^{-1}$ ,  $T$  (room temperature) is 298.15 Kelvin, and  $K_{i_{pred}}$  is the predicted inhibitory constant. Ligand efficiency (LE) is a commonly applied parameter for selecting favorable ligands by comparing the values of average binding energy per atom [13]. The following formula was applied to calculate LE:

$$LE = -\Delta G/N$$

where LE is the ligand efficiency ( $\text{kcal mol}^{-1} \text{ non-H atom}^{-1}$ ),  $\Delta G$  is binding affinity ( $\text{kcal mol}^{-1}$ ) and  $N$  is the number of non-hydrogen atoms in the ligand.

### MOLECULAR DYNAMICS (MD) SIMULATIONS

To study the dynamic behavior of the protein complex under simulated physiological conditions, MDSs of the protein-ligand (PL) complex were performed using Desmond, which is available with Schrodinger Maestro (v12.5). The PL complex (9198 atoms) was solvated in a  $10 \times 10 \times 10 \text{ \AA}$  orthorhombic periodic Page 7/21 box built with TIP3P water molecules (Jorgensen, Chandrasekhar, Madura, Impey, & Klein, 1983). The whole system was neutralized by adding an appropriate number of counter ions. This solvated system was energy minimized and position restrained. Furthermore, 100 ns of MDS was carried out at 1 atm pressure and 300 K temperature, implementing the NPT ensemble with a recording interval of 100 ps, resulting in a total of 1000 read frames. Finally, various parameters of the MDS, such as ligand-binding site analysis, RMSD, root mean square fluctuation (RMSF), PL contacts, secondary structure element (SSE) analysis, etc., were also analyzed to check the stability, compactness, structural fluctuations and protein ligand interactions in the solvated system [12].

### CIRCULAR DICHROISM (CD) SPECTROSCOPY

The CD measurements were carried out on a Chirascan<sup>TM</sup> spectropolarimeter (USA) at 298K with a thermostatically controlled cell holder attached to a water bath with an accuracy of  $\pm 0.1 \text{ K}$ . The spectra were scanned in far-UV range from 200-260 nm in a quartz optical cell with a path length of 0.1 cm. The concentration of HSA used was  $5 \mu\text{M}$ , and the buffer signal was subtracted from protein to get the correct CD spectrum of protein. The raw CD data were converted to mean residual ellipticity  $[\Theta]$  ( $\text{deg cm}^2 \text{ dmol}^{-1}$ ) i.e., concentration independent parameters by utilizing following equation.

$$MRE = \frac{M_0 \theta \lambda}{10/C}$$

Where  $M_0$  is the mean residue weight of the protein,  $\theta \lambda$  is the observed ellipticity in millidegrees at wavelength  $\lambda$ ,  $C$  is the protein concentration in  $\text{mg ml}^{-1}$  and  $l$  is the path length of the cell in centimeters. The percentage of  $\alpha$ -helical content of HSA was estimated by the ellipticity values at 208nm from the following equation.

$$\text{Helical (\%)} = \frac{-[\text{MRE}_{208} - 4000]}{33000 - 4000} \times 100 \quad [13]$$

## RESULT AND DISCUSSION

### UV-vis SPECTROSCOPY

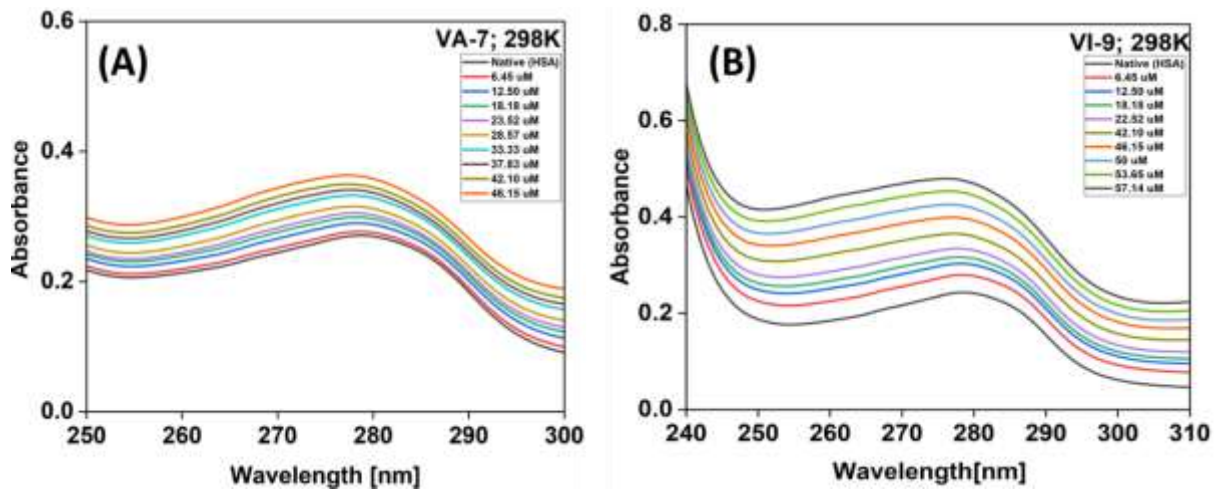


**Figure 1[A/B]. UV-vis spectra and of HSA (5µM) with different concentration of VA-7/VI-9 at 298K**

One easy way to look into the structural alterations in proteins brought about by ligand binding is to employ UV-vis spectroscopy. In order to comprehend how VA-7/VI-9 binds to HSA, the absorption spectra of HSA at various VA-7/VI-9 concentrations were examined in this work. Figure 1[A/B] displays the HSA absorption spectra as VA-7/VI-9 concentration increases (6.45–46.15 µM). Without any discernible changes in peak location at 279 nm, the absorption peak of HSA at 279 nm grew steadily with the slow addition of VA-7/VI-9. The fact that the VA-7/VI-9 does not exhibit an absorption peak in the 279 nm region confirms that the HSA – VA-7/VI-9 complex formation was the cause of the rise in absorbance at 279 nm.

### DETERMINATION OF BINDING CONSTANT

The absorbance values of HSA were measured at 279 nm and two different temperatures (298K and 308K) in the presence and absence of VA-7/VI-9 in order to calculate the binding constant.  $1/(A-A_0)$  versus  $1/\text{concentration}$  was plotted on the graph using the Benesi-Hildebrand equation.

$$\frac{1}{A - A_0} = \frac{1}{A_{max} - A_0} + \frac{1}{A_{max} - A_0} \times \frac{1}{Kb [Q]}$$

Where  $A_0$  and  $A$  are the absorbance of HSA in the absence and presence of VA-7/VI-9 respectively.  $[Q]$  is the concentration of VA-7/VI-9 and  $A_{max}$  is the absorbance at saturation i.e. at  $[Q]$  max. The absorbance data were used to make a plot of  $1/(A-A_0)$  versus  $1/\text{VA-7} \& \text{VI-9}$  concentration for given temperatures. Fig 2 (A/B). The association constant  $K_b$  was calculated from the ratio of intercept to slope where the correlation coefficient ( $R^2$ ) value observed was 0.99. The value is summarised in Table 1. For VA-7 the values of  $K_b$  were found to be  $5.25 \times 10^{-2} \text{ L Mol}^{-1}$  and  $4.68 \times 10^{-2} \text{ L Mol}^{-1}$  at 298K and 308K. For VI-9 the values of  $K_b$  were found to be  $9.4 \times 10^{-3} \text{ L Mol}^{-1}$  and  $0.2 \times 10^{-3} \text{ L Mol}^{-1}$  at 298K and 308K respectively. The lower  $K_b$  value at higher temperature shows less binding of VA-7/VI-9 with HSA at higher temperature. Further, the decrease in  $K_b$  at high temperature provides an idea about the static type of quenching mechanism in the interaction system which was further confirmed by time resolve fluorescence and steady state fluorescence. Comparison of binding constants was made in three aspects:

- those for various drugs bound to the same protein
- those for binding to HSA

- those for serum albumin with those for tryptophan.

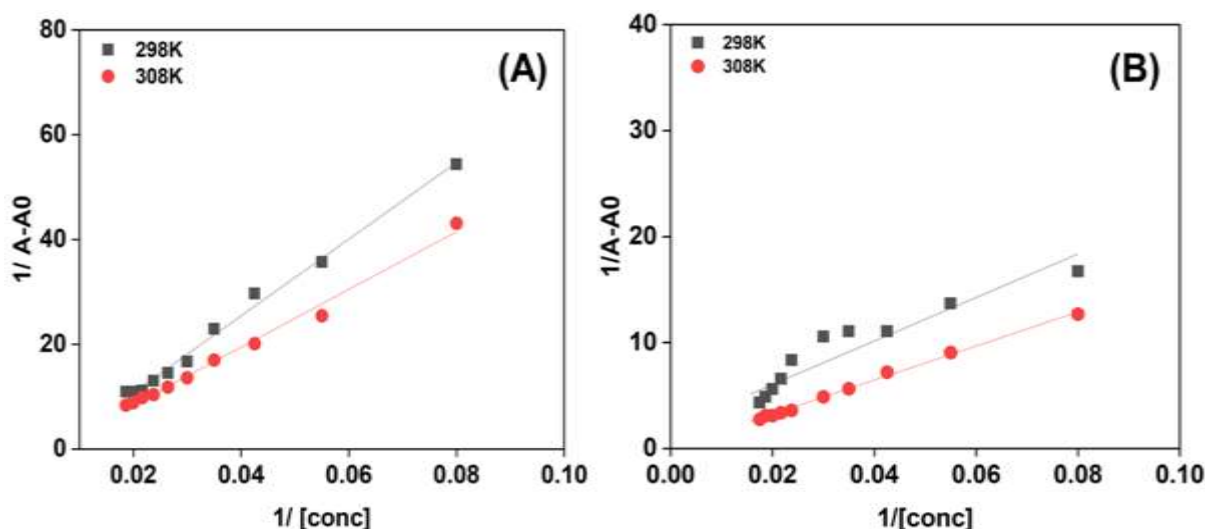


Fig 2. (A/B) Double reciprocal plot of VA-7/VI-9 298K and 308K.

### ANALYSIS OF THERMODYNAMIC PARAMETERS

To determine the type of interaction involved between HSA and VA-/VI-9, we study various thermodynamics parameters such as Gibbs free energy ( $\Delta G$ ), enthalpy change ( $\Delta H$ ) and entropy change ( $\Delta S$ ). Generally, four types of non-covalent interactions, viz. hydrophobic interactions, electrostatic forces, hydrogen bonds, and van der Waal forces play major role in ligand interaction [9]. The ( $\Delta_r H$ ) and ( $\Delta_r S$ ) determine the signs and magnitude of the binding free energy. Based on the sign and magnitude of ( $\Delta_r H$ ) and ( $\Delta_r S$ ), thermodynamics parameters of binding process could be calculated. The UV-Vis absorption data at two temperatures (298K and 308K) were used to elicit the thermodynamics parameters by the following equation [9].

$$\Delta_r H = \frac{2.303RT_1T_2}{T_2 - T_1} \log \frac{Kb_2}{Kb_1}$$

$$\Delta_r G = -2.303RT \log Kb$$

$$\Delta_r G = \Delta_r H - T\Delta_r S$$

Where  $Kb_1$  and  $Kb_2$  are the binding constant of protein – ligand complex at 298K and 308K, respectively,  $R$  is the universal constant ( $8.314 \text{ J K}^{-1}\text{mol}^{-1}$ ) and  $T$  is the experimental temperature. Herein, as shown in Table 1 the negative values of  $\Delta_r H$ , and  $\Delta_r S$  revealed that the interaction in the VA-7 system is favored by hydrogen bonding and van der Waals forces. The negative value of  $\Delta_r H$  indicated that the formation of drug-protein complex formation and the process is exothermic and enthalpy driven. In VI-9 the positive value of  $\Delta_r H$  indicated that the process is endothermic driven.

**Table 1, Binding constant Kb, R<sup>2</sup>, Δ<sub>r</sub>G, Δ<sub>r</sub>H and Δ<sub>r</sub>S**

COMPOUNDS	TEMP(K)	K <sub>b</sub> (10 <sup>-3</sup> LMol <sup>-1</sup> )	R <sup>2</sup>	Δ <sub>r</sub> G(KJMol <sup>-1</sup> )	Δ <sub>r</sub> H (KJ Mol <sup>-1</sup> )	Δ <sub>r</sub> S(Jmol <sup>-1</sup> K <sup>-1</sup> )
VA-7	298	5.27	0.99	13.00	-9.663	-0076
	308	4.68	0.99	13.23		
VI-9	298	9.4	0.89	4.0	293.77	0.97
	308	0.2	0.99	5.5		

### STEADY – STATE FLUORESCENCE

Fluorescence spectroscopy is an ideal and powerful methodology for the potent and reliable study of protein–ligand interactions. [10] Steady state fluorescence spectroscopy is a sensitive technique to obtain information about the binding strength, binding modes and the number of binding sites in ligand – protein interaction. Fluorescence quenching is the decrease of the quantum yield of fluorescence from a fluorophore induced by a variety of molecular interactions with quencher molecule, including exciting-state reactions, molecular rearrangements, energy transfer, ground-state complex formation and collisional quenching processes. Quenching can be classified as either dynamic or static quenching by different mechanisms [11]. Due to the presence of intrinsic fluorophores such as Trp, Tyr, and Phe, serum proteins like HSA exhibit a fluorescence emission band. In this instance, the HSA revealed a distinctive emission band at 324 nm, as seen in Figure 3 (A/B). The gradual addition of different concentrations of VA-7/VI-9 without causing any variation in the fluorescence intensity of HSA indicates that complex formation is responsible for the interaction between HSA and VA-7/VI-9. Additionally, when VA-7/VI-9 was titrated on HSA, some additional peaks were noticed as a result of the characteristic fluorescence peak that the VA-7/VI-9 displayed at 327 nm.

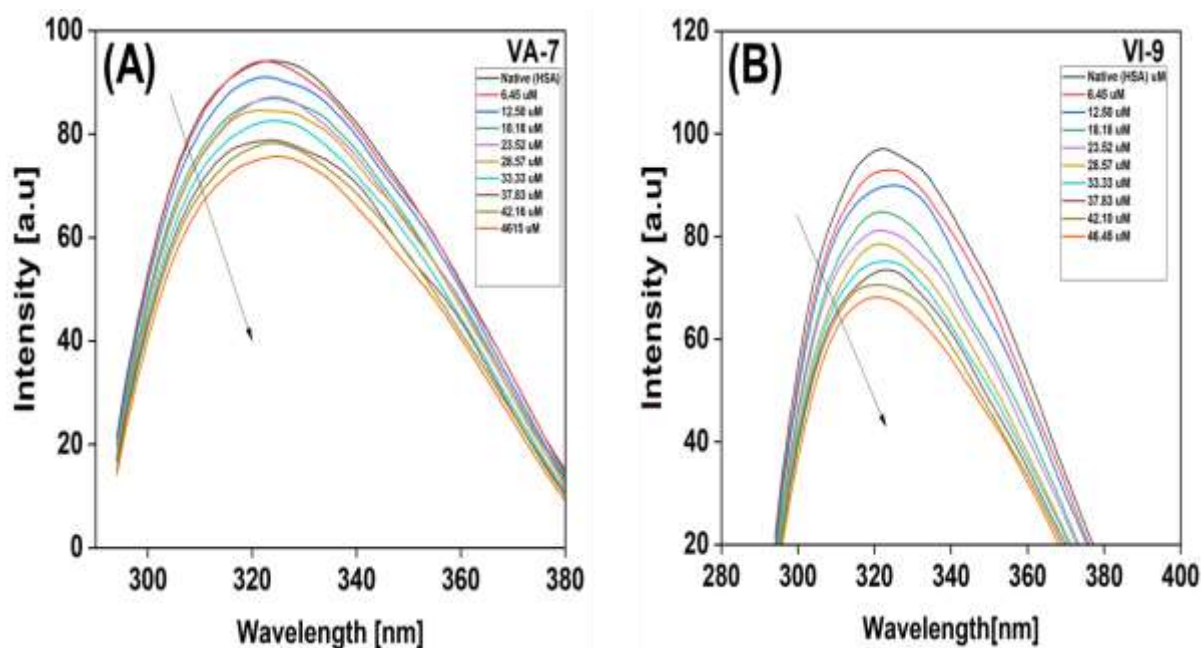


**Figure 3[A/B]. Fluorescence quenching spectra of HSA (5 μM) with different concentration of VA-7/VI-9 at 298K.**

**INTRINSIC EMISSION QUENCHING, BINDING CONSTANT AND NUMBER OF BINDING SITES.**

The quenching constant  $K_{sv}$  [Stern-Volmer constant], which is used as a measure of binding affinity., which indicates the sensitivity of the fluorophore to a quencher was calculated using Stern-Volmer equation

where  $F_0$  is the fluorescence intensity of HSA in the presence of VA-7/VI-9,  $Q$  is the VA-7/VI-9 concentration,  $K_q$  stands for quenching rate constant and  $\tau_0$  is the average lifetime of protein without quencher, and its reported value is  $10^{-8}$  s. Stern-Volmer constant, which is used as a measure of binding affinity. [12]

$$\frac{F_0}{F} = 1 + K_{sv}[Q] = 1 + K_q\tau_0[Q]$$

The plot of Stern – Volmer equation in the presence of varying concentrations of VA-7/VI-9 is depicted in Figure 4(A/B). As evident from this figure, the plot of  $F_0/F$  versus [VA-7/VI-9] has a linear relationship. For, VA-7 the Stern – Volmer quenching constant ( $K_{sv}$ ) was determined from the slope and intercept of the linear curve found to be  $0.01253 \pm 40711$ . For, VI-9 Stern – Volmer quenching constant ( $K_{sv}$ ) is found to be  $1.05824 \pm 0.0$  at 298K. The calculated value of  $K_q$  for HSA – VA-7 and VI-9 complex is  $1.25 \times 10^{10}$  and  $1.05 \times 10^8$  which is lesser than the bimolecular quenching constant i.e.,  $2.0 \times 10^8 \text{ M}^{-1}\text{s}^{-1}$ . The  $K_q$  values of both drug indicates the static quenching mechanism in the HSA- VA-7/VI-9 complex formation. Static quenching was further confirmed by time resolve fluorescence decay study. Binding constant  $K_b$  and the number and the number of binding sites ( $n$ ) were evaluated by employing following equation [12].

$$\log \frac{F_0 - F}{F} = \log K_b + n \log [Q]$$

$F_0$ ,  $F$  and  $[Q]$  have the same meaning as in equation 1. The double log plot between  $\log F_0/F$  and  $\log [VA-7/VI-9]$  at 298K for HSA shows a straight line figure 5 (A/B). For VA-7, the intercept and slope obtained from this plot gave the value of  $K_b$  which is  $37.7068 \text{ Lmol}^{-1}$  and the value of  $n$  for VA-7 –HSA complex is significantly 1 signifying the presence of one binding site on HSA for VA-7. For VI-9, the intercept and slope obtained from this plot gave the value of  $K_b$  which is  $37.229 \text{ Lmol}^{-1}$  and the value of  $n$  for VI-9 – HSA complex is significantly 1 signify the presence of one binding site on HSA for VI-9.

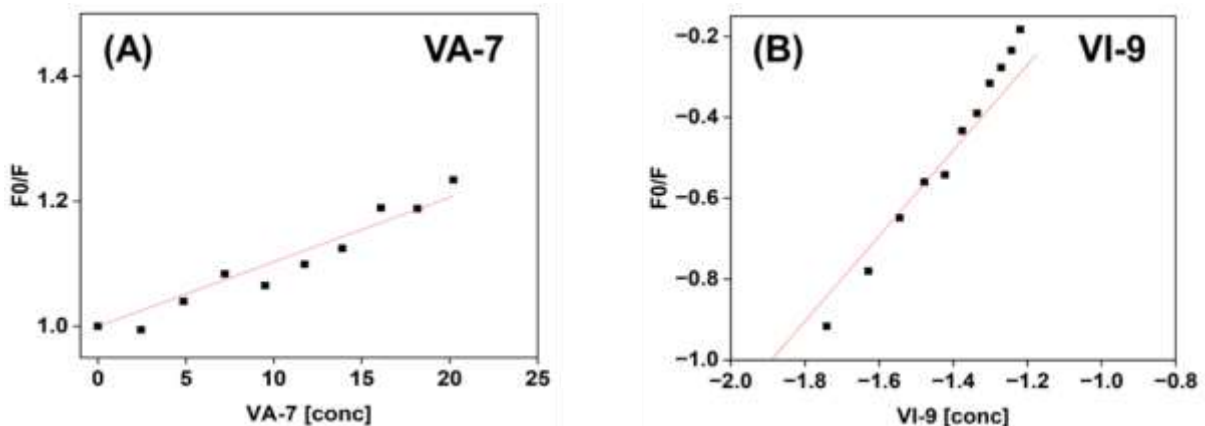


**Figure 4. [A/B] Stern – Volmer plots for the quenching of HSA by VA-7/VI-9.**

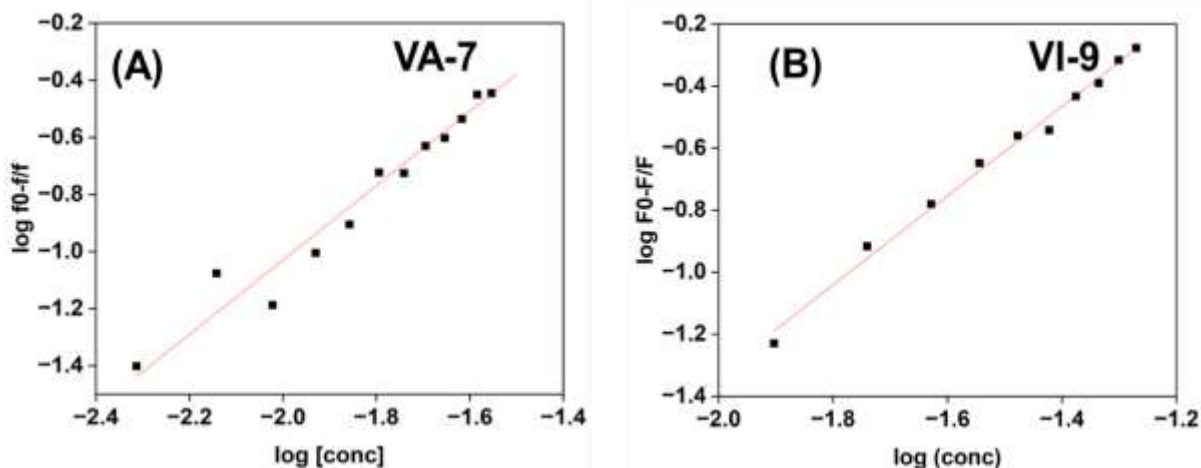


Figure 5. [A/B] Plot of  $\log (F_0-F)/F$  versus  $\log$  for the quenching HSA by VA-7/VI-9 at 298K

### SYNCHRONOUS FLUORESCENCE

To confirm the binding of VA-7/VI-9 with HSA, synchronous fluorescence is used as an additional approach. Synchronous fluorescence spectroscopy (SFS) is a technique that has been used to study the microenvironment of amino acid residues of biomolecules under various physiological conditions. It involves scanning the excitation and emission monochromators of a fluorimeter simultaneously while maintaining a fixed wavelength difference ( $\Delta\lambda$ ) between them. [13]. Therefore, we fixed  $\Delta\lambda$  ( $\lambda_{em}-\lambda_{ex}$ ) = 60 nm for Trp and 15 nm for Tyr in order to measure their emission spectra in this case. The synchronized fluorescence spectra of HSA at various VA-7 concentrations are shown in Figure 6(A/B). The fluorescence intensity of Tyr and Trp steadily reduced without shifting when VI-9 was added, as shown in Figure 7(A/B). The drop was more pronounced in the case of Trp than Tyr, indicating that there were more microenvironmental changes in the Trp C residues of HSA when VA-7/VI-9 was present.

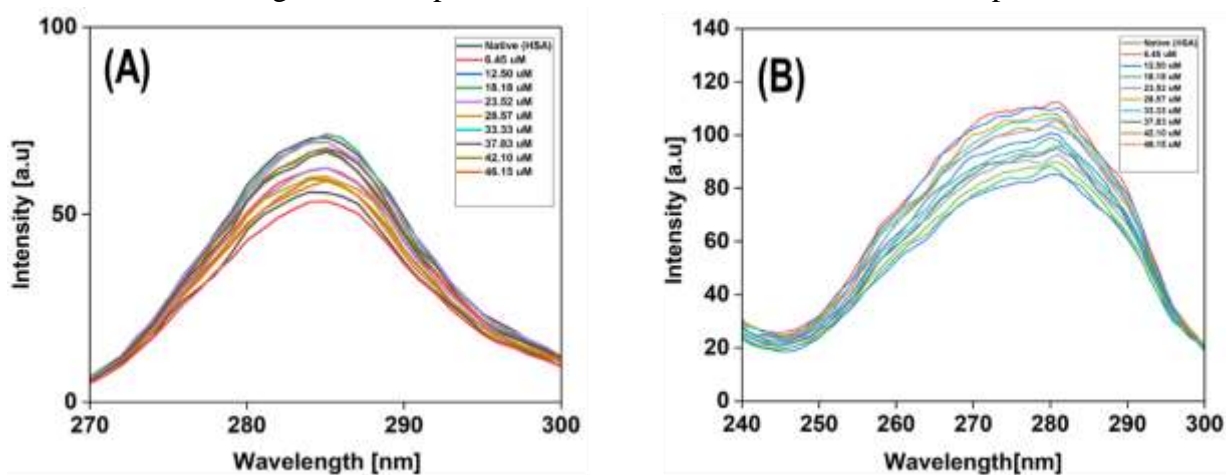


Fig 6. [A/B] Synchronous fluorescence spectra as a function of VA-7 concentration at  $\Delta\lambda=15\text{nm}$  and  $\Delta\lambda=60\text{nm}$  at 298K.

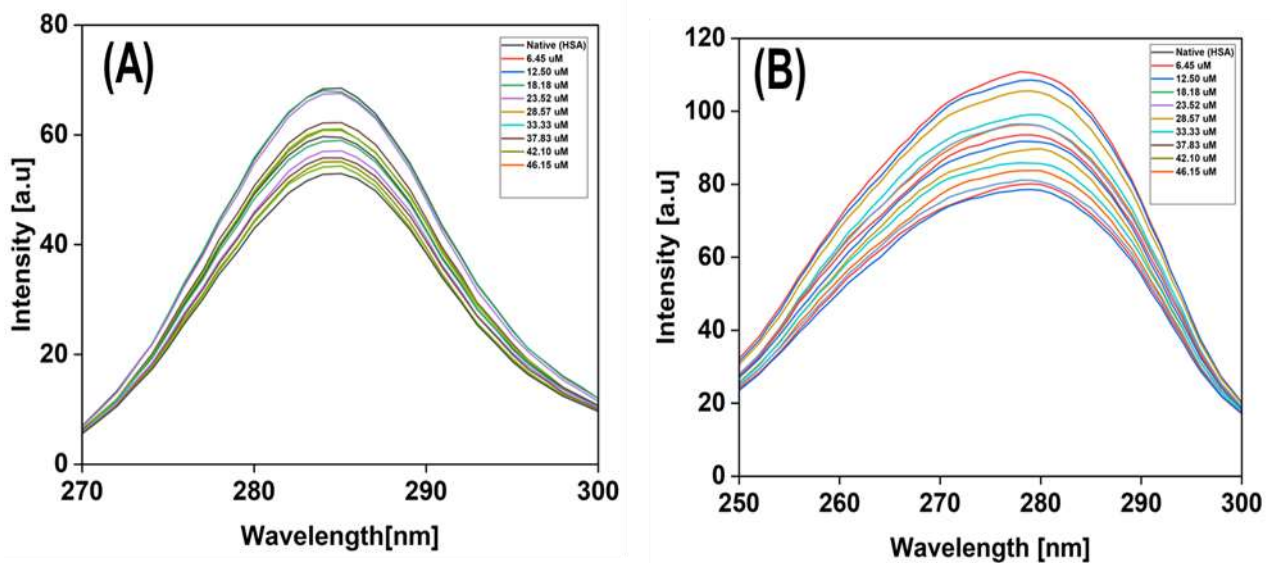


Fig 7.[A/B] Synchronous fluorescence spectra as a function of VI-9 concentration at  $\Delta\lambda=15\text{nm}$  and  $\Delta\lambda=60\text{nm}$  at 298K.

### THREE –DIMENSIONAL (3D) FLUORESCENCE

Protein structures can be thoroughly investigated using three-dimensional fluorescence spectroscopy. The interference of VA-7/VI-9 with the HSA spatial structure is examined using the 3D fluorescence spectra, which may reveal structural alterations in the HSA. [14]. The residues' maximum emission wavelength and fluorescence intensity revealed a strong correlation with the microenvironment's polarity. [15]. Furthermore, some significant data regarding the conformational changes in proteins in the presence of ligands is also provided by the contour plots. The natural HSA's 3D fluorescence is seen in Figure 8(A). As seen, the first order Rayleigh scattering peak is represented by peak A ( $\lambda_{em}=\lambda_{ex}$ ), and the second order scattering peak is shown by peak B ( $2\lambda_{em}-\lambda_{ex}$ ). The main fluorescence peak under study is Peak 1 ( $\lambda_{ex} = 280.0 \text{ nm}$ ,  $\lambda_{em} = 350.0 \text{ nm}$ ), which displays the spectral properties of tryptophan and tyrosine residues. Peak 2's excitation wavelength was measured at 225 nm, and this was mostly ascribed to the protein's distinctive polypeptide backbone structure's  $n\rightarrow\pi^*$  transition [16]. In this work, peak A increases whereas peak B dramatically lowers upon binding to VI-9 (Figure 8C) and VA-7 (Figure 8B). This can be explained by the development of a complex involving a modification in the structure of the protein. Furthermore, upon the addition of ligands, peak 1 and peak 2's fluorescence intensities dropped. The native protein's  $\lambda_{max}$  did not significantly shift in either case during the current investigation. However, the substantial drop in peak 1 and peak 2 intensities indicates that, although ligand concentrations at lower levels led to very slight structural changes in HSA, higher ligand concentrations resulted in a large disturbance in the protein. The corresponding contour spectra also revealed a significant alteration. Finally, VA-7 changed the less structural variation in the protein than in VI9. As a result, VA-7 is thought to interact with the environment better than VI-9.

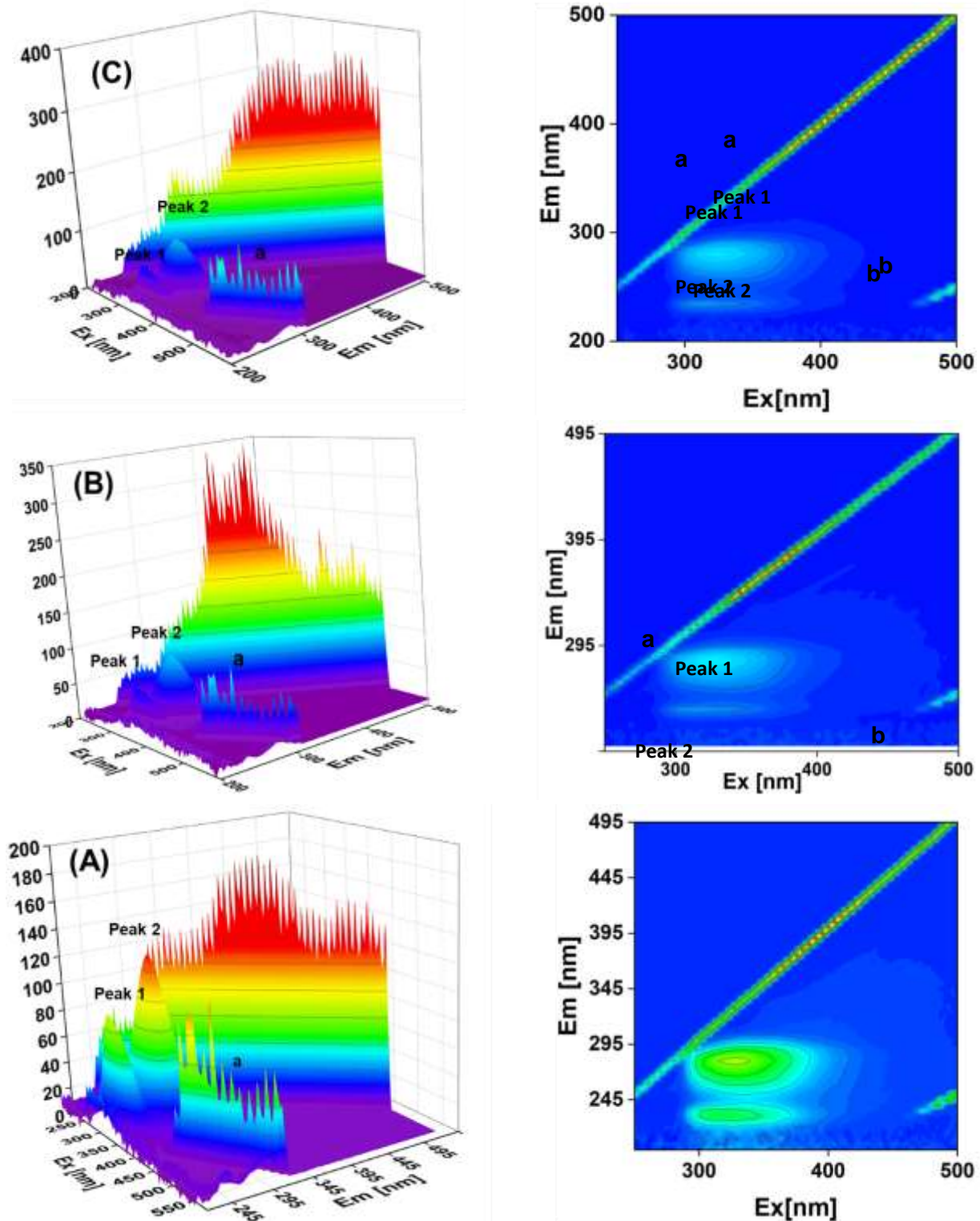


Fig 8[A/B/C]. 3D fluorescence and contour maps of (A) HSA (human serum albumin), (B) HSA-VA-7 complex, and (C) HSA-VI-9 complex

### TIME – RESOLVE FLUORESCENCE SPECTROSCOPY

The method of time-resolved fluorescence spectroscopy is commonly employed to differentiate between static and dynamic quenching mechanisms. When a protein (fluorophore) interacts with a drug (quencher) in a dynamic quenching process, its average life span decreases, whereas in a static quenching process,

the formation of a non-fluorescent complex has no effect on the average life span of an uncomplexed fluorophore [17]. This difference between the two mechanisms is made. When HSA was excited at 279 nm at 298 K, time-resolved fluorescence spectra of the native HSA were acquired both before and after the addition of VA-7/VI-9. Furthermore, Table 2 displays the average life time parameters derived from multi exponential fitting of the VA-7 decay profiles, whereas Table 3 displays the average life time parameters extracted from the VI-9 decay profiles. The native HSA's  $\tau_{avg}$  value of 5.44 ns is in good agreement with the literature that is currently accessible [17].

It was noted that the  $\tau_{avg}$  value did not change much as the concentration of VA-7/V-9 increased. These findings unequivocally demonstrated that the HSA-VA-7/VI-9 binding mechanism was dominated by static quenching. Here, Figure 11(A/B) displays the demonstrative life-time decay curves of HSA's Trp residues in the presence and absence of VA-7/VI-9. In order to bolster the quenching process even further, we also computed the ratio of  $\tau/\tau_{avg}$  of VA-7/VI9 and plotted it in Fig. 12(A/B). Static quenching is further confirmed by the value being nearly constant and equivalent to one.

**Table 2, Fluorescence decay of HSA with different concentration of VA-7.**

VA-7( $\mu\text{M}$ )	$\tau_1(\text{ns})$	$\tau_2(\text{ns})$	$\tau_3(\text{ns})$	$\alpha_1(\%)$	$\alpha_2(\%)$	$\alpha_3(\%)$	$\tau_{avg}(\text{ns})$	$\chi^2$
0.00	2.56	6.54	0.77	39.23	47.26	13.51	5.44	1.03
6.45	2.81	6.86	0.80	43.32	47.19	15.6	5.50	0.95
23.52	2.66	6.68	0.71	42.51	42.12	15.37	5.39	0.98
37.83	2.95	6.94	0.86	43.81	36.18	19.95	5.37	1.00
50	2.53	6.47	0.69	42.85	40.21	16.94	5.17	1.15

**Table 3, Fluorescence decay of HSA with different concentration of VI-9.**

VI-9( $\mu\text{M}$ )	$\tau_1(\text{ns})$	$\tau_2(\text{ns})$	$\tau_3(\text{ns})$	$\alpha_1(\%)$	$\alpha_2(\%)$	$\alpha_3(\%)$	$\tau_{avg}(\text{ns})$	$\chi^2$
0.00	2.56	6.54	0.77	39.23	47.26	13.51	5.44	1.03
6.45	2.60	6.78	0.59	42.25	43.61	14.14	5.55	1.03
23.52	2.69	6.81	0.73	42.43	42.47	15.10	5.51	1.03
37.83	2.09	6.10	0.35	40.32	39.76	19.92	4.97	1.07
50	2.39	6.45	0.53	42.82	43.43	13.76	5.27	1.16

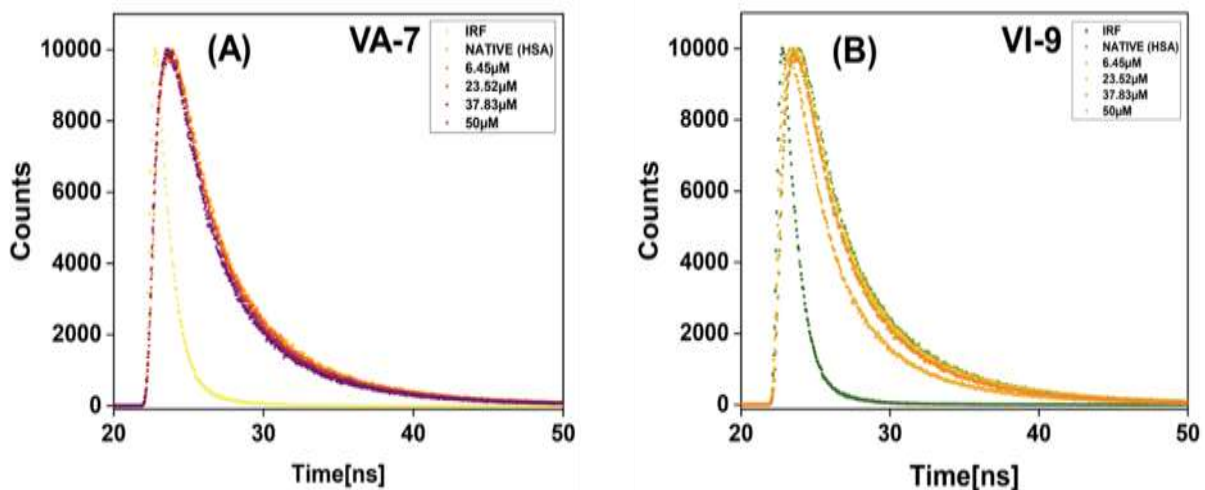


**Figure 11. (A/B) Fluorescence decay HSA with increasing concentration of VA-7/VI-9**

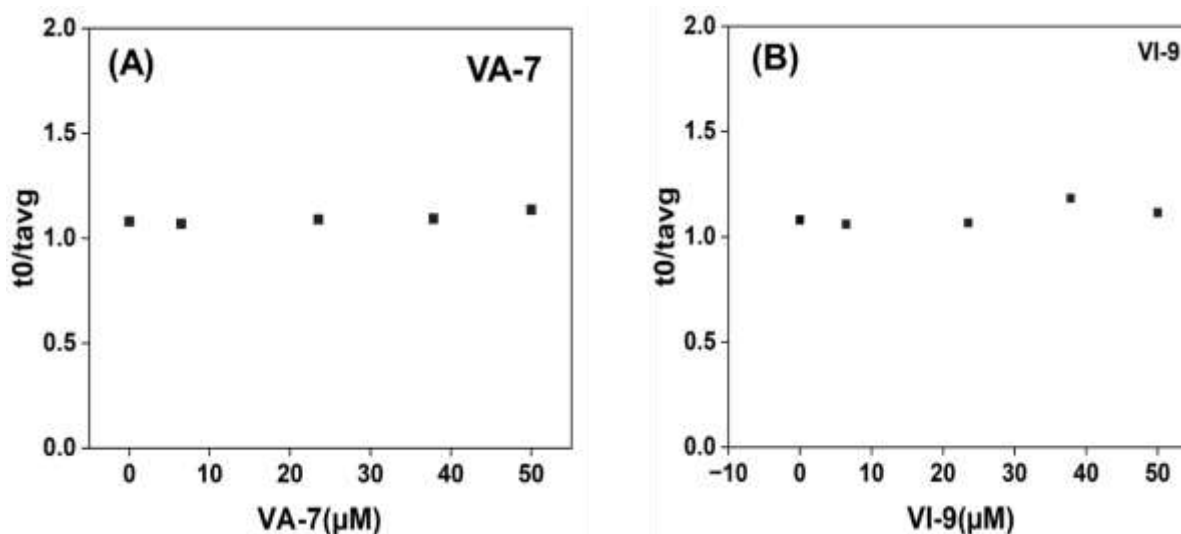


Figure 12.(A/B) Plot  $\tau/\tau_{avg}$  as a function of VA-7/VI-9 at 298K .

### MOLECULAR DOCKING

Compound VA-7 and VI-9 were subjected to docking analysis, they presented a binding affinity value of -8.8 kcal/Mol and -8.9 kcal/Mol, respectively towards the receptor HSA.. Interaction analysis of the all possible docked conformers of both the compounds was carried out to investigate their binding pattern and possible interactions towards the HSA binding pocket.

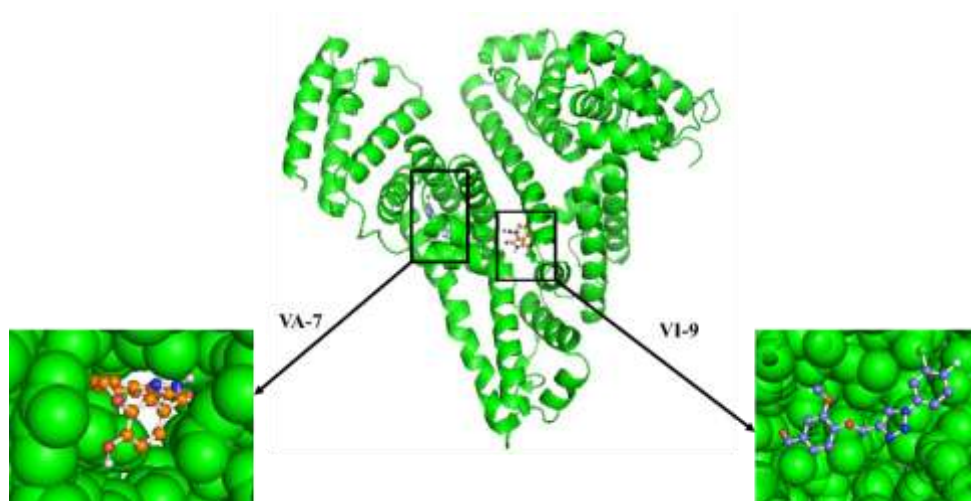
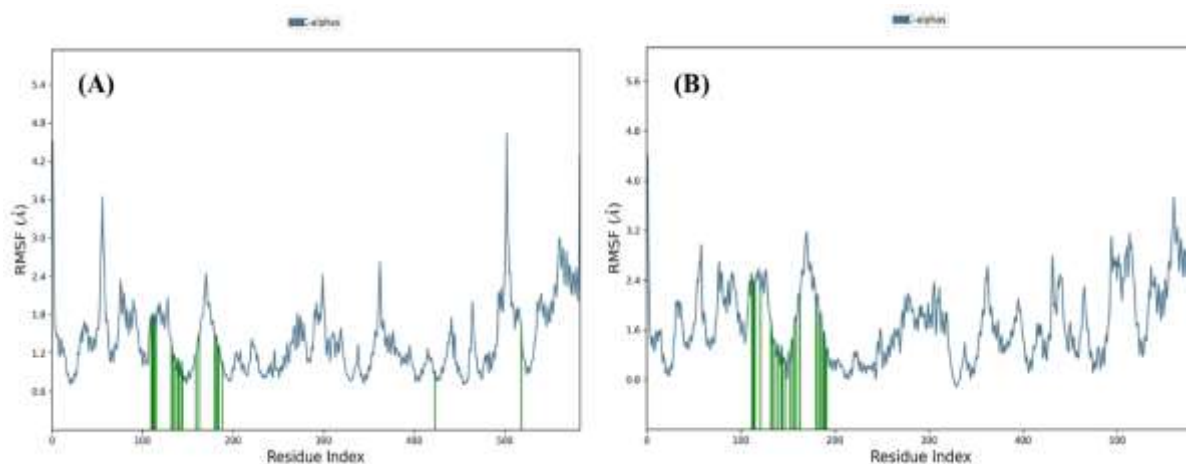


Fig 13. Binding pattern and interaction of VA-7/VI-9 with HSA

### MOLECULAR DYNAMIC (MD) SIMULATION

In a molecular dynamics simulation, the average displacement of a chosen set of atoms over several frames in relation to a reference frame is measured using the Root Mean Square Deviation (RMSD) metric. Each frame is first aligned with the reference frame, and then the positions of the chosen atoms are used to calculate the RMSD for each frame. This procedure sheds light on how the structures of ligands and proteins alter during the simulation. Tracking RMSD over time for proteins can provide insights on their structural stability. Variations in the RMSD show if the simulation has reached equilibrium, with small changes generally considered acceptable for stable, compact proteins. Considerable structural changes are suggested by significant variances. Furthermore, convergence is indicated by constant RMSD values at

the end of the simulation, whereas persistent trends point to insufficient simulation time. The protein HSA fluctuation pattern in Figure 14(A/B) is nearly identical to that of compound VA-7/VI-9, with a nearly constant small variation in their RMSD values, indicating that the protein and compound are in a stable complex. It is evident from the reduced RMSD values of VA-7/VI-9 relative to the protein that the ligand stayed confined within the protein's binding pocket rather than diffusing out.



**Figure 14(A/B). Protein (HSA)-ligand (VA-7/VI-9) RMSD graph.**

To analyze local alterations along a protein chain, one technique is to employ the Root Mean Square Fluctuation (RMSF). The HSA protein's sections that fluctuated the most during the simulation are indicated by peaks in the RMSF plot in figure 15(A/B), with terminal areas usually fluctuating more than secondary structural elements like alpha helices and beta strands. Residues interacting with the ligand are indicated on the plot with green color for additional analysis, and secondary structural elements are recognized and highlighted.

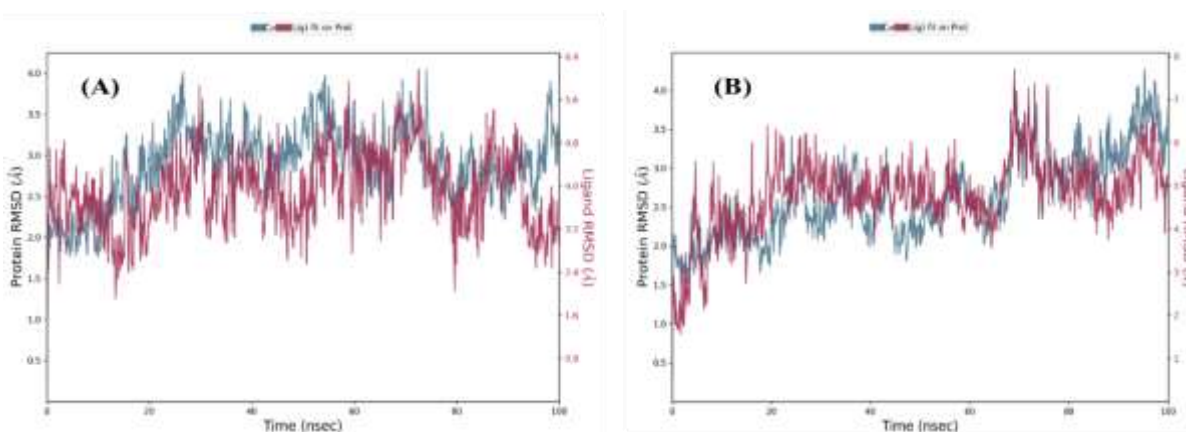


**Figure 15(A/B). Protein (HSA)-ligand (VA-7/VI-9) RMSD graph.**

### Protein-ligand contact

The interactions between proteins and ligands are tracked and classified into different categories throughout a molecular dynamics simulation. These interactions include hydrogen bonds, hydrophobic interactions, ionic interactions, and water bridges. Figure 16(A/B) plots these interactions. Subtypes such

as backbone acceptor, p-Cation, and protein-water bridges are further differentiated into each kind. With numbers normalized to show the fraction of time each interaction persists, the plot shows the prevalence of these interactions over the trajectory. Tyr62, for example, demonstrated hydrogen bonding for 50% of the simulation duration. Among all, hydrophobic forces were discovered to be the important interactions. A thorough understanding of these protein-ligand interactions is vital for molecular research and drug design, as they are critical for drug selectivity and binding affinity.

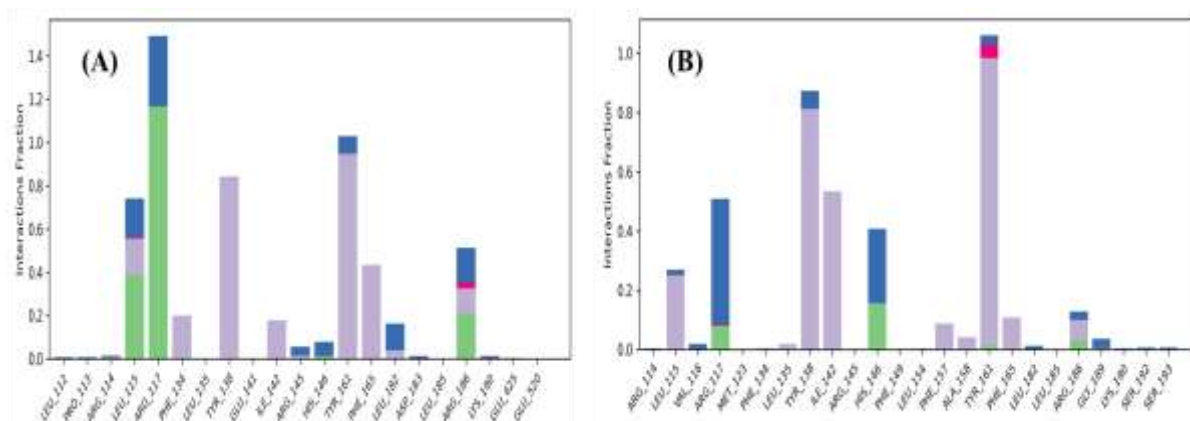


Figure 16(A/B). Histogram showing protein (HSA)-ligand(VA-7/VI-9) contacts

### CIRCULAR DICHROISM (CD)

CD has been widely used to monitor the secondary structural changes of proteins during the ligand–protein complexation. The far-UV region (200– 260 nm) of the CD spectrum in solution, corresponding to peptide bond absorption, was employed to get insight on the possible influence of VA-7/VI-9 binding on the secondary structure of HSA. The CD spectra of HSA exhibited two negative bands at 214 and 228 nm, appeared due to the  $\alpha$ -helical and  $\beta$ -sheet structure of protein, respectively. The CD curves of HSA in the presence and absence of cadmium acetate were similar in shape, indicating that  $\alpha$ -helix is still the main components of HSA secondary structure. As evident from Figure 17(A/B), interaction between VA-7/VI-9 and HSA resulted in a reduction of  $\alpha$ -helical structures of HSA, implying that VA-7/VI-9 might bind with the amino acid residues of the main polypeptide chain of protein and destroyed their hydrogen bonding networks. the content of  $\alpha$ -helix content in HSA could be determined. The formation of VA-7–HSA complex causes the change of  $\alpha$ -helical content from 81.2% in free HSA to 73.19%,75.43% and 32.80% when the concentration of VA-7 increases to 2.47 -16.09  $\mu$ M . The formation of VI-9–HSA complex causes the change of  $\alpha$ -helical content from 81.2% in free HSA to 76.26%,64.17% and 36.01% when the concentration of VI-9 increases to 2.47 -16.09  $\mu$ M . Therefore, the addition of VA-7/VI-9 had a relatively minor impact on the shape of the HSA CD spectrum, indicating a partial transformation from a  $\alpha$ -helix structure.

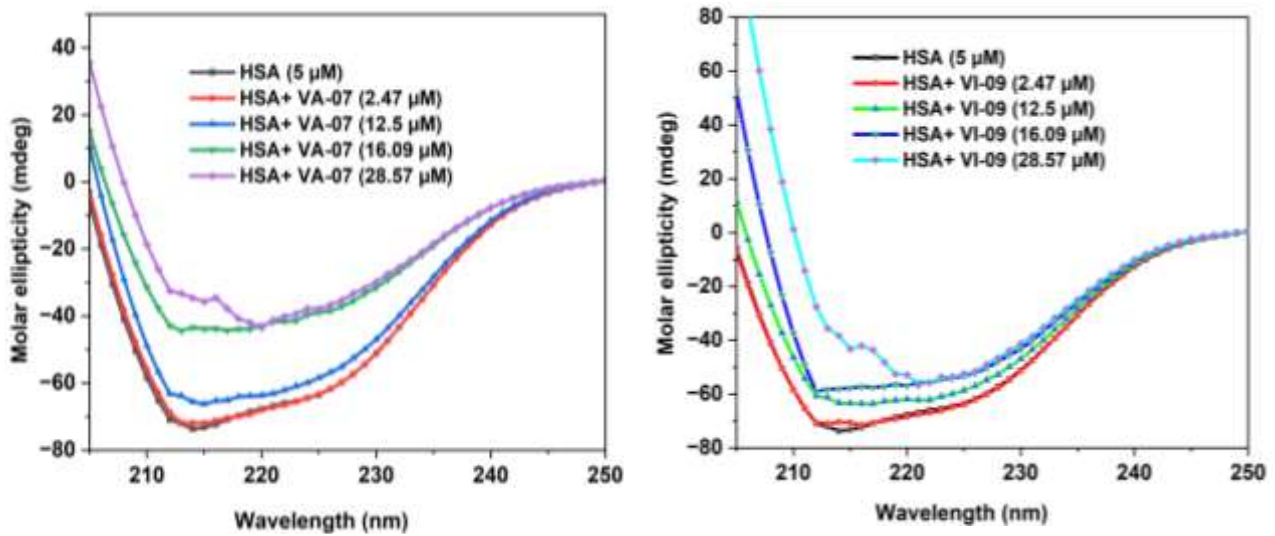


Fig 17(A/B) CD (circular dichroism) spectra of HSA (human serum albumin) on interaction with VA-7 and VI-9.

Sample	$\alpha$ -Helix (%)
HSA	81.2
HSA + VA-07 (2.47 $\mu$ M)	73.19
HSA + VA-07 (12.5 $\mu$ M)	75.43
HSA + VA-07 (16.09 $\mu$ M)	32.80

Table 4. Calculated percentage of  $\alpha$ -helical structure of protein obtained through CD table.

Table 5. Calculated percentage of  $\alpha$ -helical structure of protein obtained through CD table.

Sample	$\alpha$ -Helix (%)
HSA	81.2
HSA + VI-09 (2.47 $\mu$ M)	76.26
HSA + VI-09 (12.5 $\mu$ M)	64.17
HSA + VI-09 (16.09 $\mu$ M)	36.01

## CONCLUSION

We examine the mechanism of interaction between VA-7/VI-9 and HSA, two possible anti-cancerous drugs, utilizing a variety of spectroscopic approaches, molecular docking, binding free energy calculations, and MD modelling. Our research unequivocally demonstrates that VA-7 linked to VI-9 and subdomain II A in the cleft between subdomain IIIA. The chemicals bind with HSA in an endothermic/exothermic and enthalpy-driven manner, according to the thermodynamic parameters and binding constant. The ligand binding did not change the Trp and Tyr environments. Both the HSA VA-7 and HSA VI-9 complexes involved static quenching, as demonstrated by the steady-state and time-resolved data. There is no greater distorting effect between VA-7 and VI-9 in the CD results. Additional

research using molecular docking of VA-7/VI-9 demonstrated the connection through van der Waals forces and hydrogen bonds. The protein does not display any aberrant structural changes when VA-7/VI-9 is present, according to MD modelling. Finally, it was discovered that VA-7 binding was more reliable and significant for the drug's transportation and metabolism. In summary, the study offers a comparative examination of the pharmacology of the selected probable anti-cancerous substance, which may be useful in comprehending the drug-like efficiency of their pharmacology.

## REFERENCES

1. Chunarkar-Patil, Pritee, et al. "Anticancer Drug Discovery Based on Natural Products: From Computational Approaches to Clinical Studies." *Biomedicines* 12.1 (2024): 201.
2. Kabir, Md Zahirul, et al. "Decoding the intermolecular recognition mode of a potent anticancer drug, abiraterone with human serum albumin: Assessments through spectroscopic and computational techniques." *Journal of Molecular Structure* 1302 (2024): 137509.
3. Meegan, Mary J., and Niamh M. O'Boyle. "Special Issue "Anticancer Drugs 2021"." *Pharmaceuticals* 15.4 (2022): 479.
4. Moudi, M.; Go, R.; Yien, C.Y.S.; Nazre, M. Vinca Alkaloids. *Int. J. Prev. Med.* 2013, 4, 1231–1235.
5. Paul, A.; Acharya, K.; Chakraborty, N. Biosynthesis, Extraction, Detection and Pharmacological Attributes of Vinblastine and Vincristine, Two Important Chemotherapeutic Alkaloids of *Catharanthus Roseus* (L.) G. Don: A Review. *S. Afr. J. Bot.* 2023, 161, 365–376.
6. Prakobwong, S.; Gupta, S.C.; Kim, J.H.; Sung, B.; Pinlaor, P.; Hiraku, Y.; Wongkham, S.; Sripa, B.; Pinlaor, S.; Aggarwal, B.B. Curcumin Suppresses Proliferation and Induces Apoptosis in Human Biliary Cancer Cells through Modulation of Multiple Cell Signalling Pathways. *Carcinogenesis* 2011, 32, 1372–1380
7. Chidambara Murthy, K.N.; Jayaprakasha, G.K.; Patil, B.S. The Natural Alkaloid Berberine Targets Multiple Pathways to Induce Cell Death in Cultured Human Colon Cancer Cells. *Eur. J. Pharmacol.* 2012, 688, 14–21.
8. Kamat, Jayashree P., Arna Ghosh, and Thomas PA Devasagayam. "Vanillin as an antioxidant in rat liver mitochondria: inhibition of protein oxidation and lipid peroxidation induced by photosensitization." *Molecular and cellular biochemistry* 209 (2000): 47-53.
9. Mohammad T, Mathur Y, Hassan MI (2020). InstaDock: A Single-click Graphical User Interface for Molecular Docking-based Virtual High-throughput Screening. *Briefings in Bioinformatics*, 00(00): 1-8. DOI: 10.1093/bib/bbaa279
10. Hassan NM, Alhossary AA, Mu Y, Kwok CK (2017). Protein-ligand blind docking using QuickVina-W with inter-process spatio-temporal integration, *Scientific Reports*, 7(1): 1-13.
11. Trott, O. and Olson, A.J. (2010) AutoDock Vina: improving the speed and accuracy of docking with a new scoring function, efficient optimization, and multithreading. *Journal of computational chemistry*, 31(2): 455-461
12. Ahmad, Shaban, et al. "Molecular dynamics simulation and docking studies reveal NF-κB as a promising therapeutic drug target for COVID-19." (2021).
13. Chen, M., Guo, H., Liu, Y., & Zhang, Q. (2014). *Structural Changes of Human Serum Albumin Induced by Cadmium Acetate*. *Journal of Biochemical and Molecular Toxicology*,
14. Shityakov, S., & Förster, C. (2014). In silico structure-based screening of versatile P-glycoprotein inhibitors using polynomial empirical scoring functions. *Advances and Applications in Bioinformatics*

and Chemistry, **7**: 1.

15. Hopkins, A. L., Groom, C. R., & Alex, A. (2004). Ligand efficiency: a useful metric for lead selection. *Drug discovery today*, **9**(10): 430.
16. Azeem, Kashish, et al. "A multi-spectroscopic and computational simulations study to delineate the interaction between antimalarial drug hydroxychloroquine and human serum albumin." *Journal of Biomolecular Structure and Dynamics* 41.13 (2023): 6377-6393.
17. Kenoth, Roopa, and Ravi Kanth Kamlekar. "Steady-state fluorescence spectroscopy as a tool to monitor protein/ligand interactions." *Optical Spectroscopic and Microscopic Techniques: Analysis of Biological Molecules*. Singapore: Springer Nature Singapore, 2022. 35-54.
18. Ge, Feng, et al. "Study on the interaction between theasinesin and human serum albumin by fluorescence spectroscopy." *Journal of Luminescence* 130.1 (2010): 168-173.
19. Gayer, Alexey V., et al. "Evaluating the Number of Ligand Binding Sites on Protein from Tryptophan Fluorescence Quenching under Typical Experimental Conditions." *Journal of Biomedical Photonics & Engineering* 6.2 (2020).
20. Hemmateenejad, Bahram, et al. "Combined fluorescence spectroscopy and molecular modeling studies on the interaction between harmalol and human serum albumin." *Journal of pharmaceutical and biomedical analysis* 67 (2012): 201-208.
21. Zhu, Meiqing, et al. "Biointeractions of herbicide atrazine with human serum albumin: UV-Vis, fluorescence and circular dichroism approaches." *International journal of environmental research and public health* 15.1 (2018): 116.
22. Pu, Hanlin, et al. "Studies on the interaction between vincamine and human serum albumin: A spectroscopic approach." *Luminescence* 29.5 (2014): 471-479.
23. Pu, Hanlin, et al. "Studies on the interaction between vincamine and human serum albumin: A spectroscopic approach." *Luminescence* 29.5 (2014): 471-479.
24. Pawar, Suma K., and Seetharamappa Jaldappagari. "Interaction of repaglinide with bovine serum albumin: Spectroscopic and molecular docking approaches." *Journal of Pharmaceutical Analysis* 9.4 (2019): 274-283.
25. Ahmad, Shaban, et al. "Molecular dynamics simulation and docking studies reveal NF- $\kappa$ B as a promising therapeutic drug target for COVID-19." (2021).